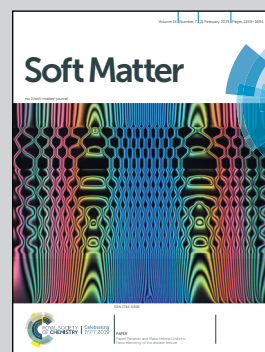**Highlighting Research from the Soft Matter Lab from the group of Giovanni Volpe.**

Active matter alters the growth dynamics of coffee rings

Active matter in a drying droplet alters the growth dynamics of coffee rings and leads to a more uniform distribution. Andac *et al.* investigate experimentally the drying process of a droplet containing suspended colloids in presence of motile bacteria, and find that the effect is particularly relevant in the case of slowly drying droplets. The experimental results are reproduced in the numerical simulation of a minimalistic model.

ROYAL SOCIETY OF CHEMISTRY | Celebrating IYPT 2019

rsc.li/soft-matter-journal

Active matter alters the growth dynamics of coffee rings†

Tugba Andac,[a] Pascal Weigmann,[a] Sabareesh K. P. Velu,[ab] Erçağ Pinçe, [ID] [ac] Giorgio Volpe, [ID] [d] Giovanni Volpe [ID] [ae] and Agnese Callegari [ID] ⋆[a]

How particles are deposited at the edge of evaporating droplets, *i.e.* the coffee ring effect, plays a crucial role in phenomena as diverse as thin-film deposition, self-assembly, and biofilm formation. Recently, microorganisms have been shown to passively exploit and alter these deposition dynamics to increase their survival chances under harshening conditions. Here, we show that, as the droplet evaporation rate slows down, bacterial mobility starts playing a major role in determining the growth dynamics of the edge of drying droplets. Such motility-induced dynamics can influence several biophysical phenomena, from the formation of biofilms to the spreading of pathogens in humid environments and on surfaces subject to periodic drying. Analogous dynamics in other active matter systems can be exploited for technological applications in printing, coating, and self-assembly, where the standard coffee-ring effect is often a nuisance.

1 Introduction

If a liquid droplet containing suspended particles is left to dry on a surface, it leaves behind a characteristic stain, which is often in the shape of a ring. This phenomenon is commonly observed when a drop of spilled coffee dries, hence the name coffee ring. In fact, this effect was already observed by Robert Brown in 1828.[1,2] The seminal work by Deegan and colleagues[3–5] showed that coffee rings arise in a wide range of situations where the contact line of an evaporating droplet is pinned.[6–10] Following work has shown that the coffee ring effect can be controlled and tuned towards more uniform distributions *via* different approaches, *e.g.*, by varying the size and shape of the suspended particles[11–15] and by introducing static or dynamic Marangoni flows.[16–22]

More recently, the coffee ring effect and its reversal have also been shown to impact microbial life.[19,23–25] In fact, microorganisms can be exposed to environments that undergo occasional or periodic drying and, therefore, might make use

of the coffee ring effect, or its absence, to optimise their chances of survival. For example, it has been shown that the production of biosurfactants by *Pseudomonas auriginosa* can reverse the coffee ring effect and produce more uniform stains upon drying.[19] Similarly, the coffee ring effect dictates inter-species competition between different strains of *Vibrio cholerae*.[25] Differences in the drying pattern exhibited by suspensions of living motile and non-motile bacteria have also been studied,[24] showing that a drying droplet containing motile bacteria leaves a spot that is disk-like, different in shape from the observed drying patterns left by a droplet of non-motile bacteria. Moreover, the evaporation of droplets containing bacteria has been studied in substrates with microfabricated pillars, showing that the microstructure of the substrate determines the shape of the dried stain and affects the spatial distribution of the bacterial species,[26] and that it is possible to discriminate between organisms with flagella and organisms without flagella by inspecting the distortion of the micropillars of the structured surface left after the evaporation.[27] Despite the fact that the shape and dynamics of drying patterns in motile and non-motile bacterial communities have been studied separately, the drying of an active system which comprises passive and active components, *i.e.*, colloids and motile bacteria, has not been studied yet to the best of our knowledge. In more realistic biological settings self-motile and non-motile elements often coexist: for example, many bacteria are motile to increase their survival chances[28–30] and passive components like dust specks or non-motile organisms are also typically simultaneously found in water droplets. A question naturally arises: what is the effect of self-motility on the dynamics occurring within a drying droplet containing both active and passive particles?

[a] *Soft Matter Lab, Department of Physics, Bilkent University, Ankara, Turkey. E-mail: callegari@fen.bilkent.edu.tr*

[b] *University of Information Science and Technology "St. Paul The Apostle", Ohrid 6000, Macedonia*

[c] *Department of Living Matter, AMOLF, Science Park 104, 1098 XC Amsterdam, The Netherlands*

[d] *Department of Chemistry, University College London, 20 Gordon Street, London WC1H 0AJ, UK*

[e] *Department of Physics, University of Gothenburg, SE-41296 Gothenburg, Sweden*

2 Experimental results

In order to answer this question, we studied the drying process of droplets containing an active bath of motile bacteria (*Escherichia coli*,[31] wild-type strain RP437 from the *E. coli* Stock Center at Yale University, cultured as described in ref. 32) in the presence of suspended colloidal particles (polystyrene microspheres with diameter $2R = 3.00 \pm 0.07$ μm, volume fraction $\phi = 0.0055$). The concentration of both bacteria and particles is the same in all the experiments. Details of the preparation of the colloidal and bacterial suspensions used in the experiments are given in the Materials and methods Appendix. As a result of random collisions with the bacteria in the suspension, the colloids feature a crossover from superdiffusive motion at short times to enhanced diffusion at long times typical of self-propelled particles, such as bacteria and other microscopic active matter systems.[33–35] To keep the bacteria alive and motile during the evaporation process, droplets were made of motility buffer containing 10 mM monobasic potassium phosphate (KH_2PO_4), 0.1 mM EDTA, 10 mM dextrose, and 0.002% Tween 20.[32]

Since the polystyrene microspheres are hydrophobic and negatively charged,[36] they produce a classic coffee-ring stain[12] upon drying when dispersed in deionized water (see Fig. S1, ESI†). The presence of electrolytes in the solution (KH_2PO_4) would naturally lead to an increased probability of flocculation and sticking due to a significant reduction of the Debye screening length. However, the presence of a chelating agent (EDTA) and of a surfactant (Tween 20) mitigates the tendency of the particles to stick to each other and to the sample slide.[37] The effect of the presence of EDTA and Tween 20 in the motility buffer on the shape of the dried stain is shown in Fig. 1a and c, where the final stain presents "holes" and "thick ridges" in its interior, evident signs of depinning in the central part of the spot. In fact, when there is only KH_2PO_4 in the buffer solution, the particles stick immediately to the glass surface, while with Tween 20 and EDTA only a fraction of the particles gets stuck, and the rest remains suspended and moves according to the flow induced by the drying. In the final stage of the evaporation, "dry holes" form in the droplet internal region and the liquid shrinks, dragging the remaining particles, in some case depinning them from the glass, and causing the formation of empty areas and thick ridges.

E. coli bacteria are Gram-negative bacteria. The shape of their body (excluding the flagella) is approximately cylindrical, about 2.6 ± 0.2 μm in length and 0.8 ± 0.1 μm in width (estimated from microscopy images of the bacteria employed in our experiments and consistent with previously reported typical sizes after cell division[31]). Their surface has a net negative charge, normally sufficient to confer colloidal stability in bulk.[37] Furthermore, the addition of non-ionic surfactants (*e.g.* Tween 20) helps minimize the adhesion of bacteria to glass surfaces[37] as those used in our experiments.

At the beginning of each evaporation experiment we deposited a 0.6 ± 0.04 μl droplet of the suspension on a glass microscope slide (25.4 mm × 76.2 mm × 1 mm), which had been previously cleaned with acetone and isopropanol, and washed with water
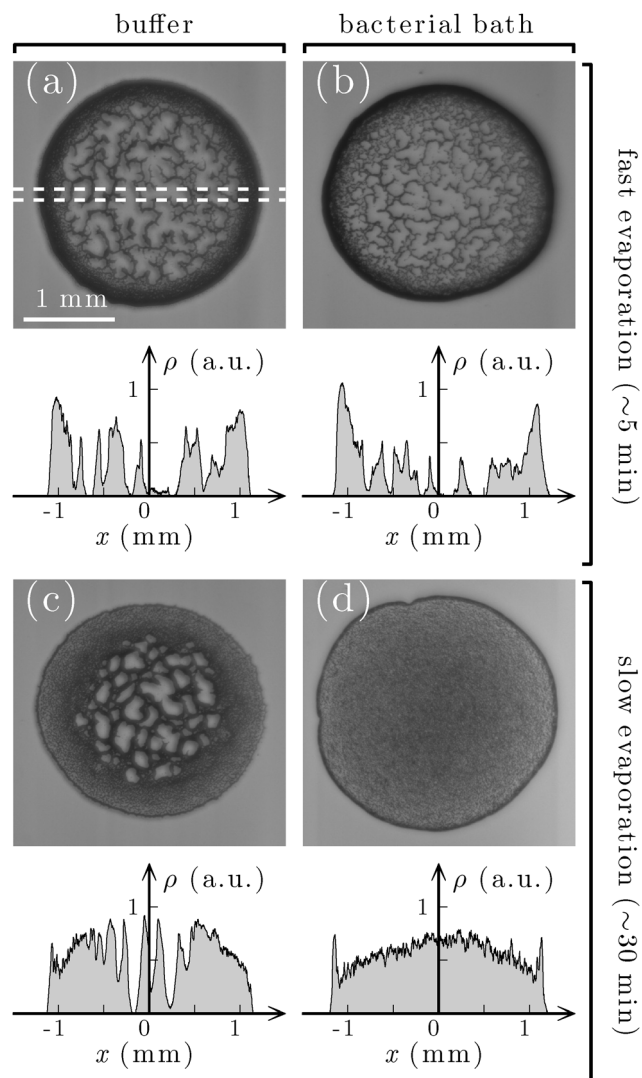

Fig. 1 Stain at the end of the evaporation with and without bacteria. Stain left behind by a droplet (a and b) after fast evaporation (~5 minutes) and (c and d) after slow evaporation (~30 minutes). The droplet is made of a buffer solution containing colloidal particles (polystyrene microsphere, diameter $2R = 3.00 \pm 0.07$ μm) (a and c) without and (b and d) with motile bacteria (*E. coli*). The plot below each panel shows the optical density of the deposit along one droplet's diameter (dashed lines in (a)) as calculated from the image inverted gray scale. (a and b) For fast evaporation, both stains share similar features. (c and d) For slow evaporation, the stain of the droplet containing bacteria features higher uniformity than all other cases. See also Supplementary Video 1 (ESI†).

after treatment with a 0.25 M NaOH solution for 5 minutes to make its surface more hydrophilic. The resulting droplet had a diameter of $2R_{drop} = 2.5 \pm 0.2$ mm, a maximum height of $h_{max} = 190 \pm 20$ μm, and a contact angle of $\theta_c = 18 \pm 1°$. The total evaporation time was 5 ± 1 minutes. We monitored the droplet evaporation using two imaging systems that projected the droplet on two CMOS cameras: the first imaging system with a 1.6×-magnification was used to record a video of the whole droplet's basal section at 5 frames per second (fps), while the second with a 40×-magnification was used to record a magnified view of the dynamics at the droplet's edge at 5 fps.

The details of the setup are provided in the Appendix and in Fig. S2 (ESI†).

As a reference for the following results, Fig. 1a shows the stain left behind by the evaporation of a droplet with only colloidal particles: because the motility buffer contains surfactants (*i.e.* Tween 20 and tryptone), the final stain shows an irregular profile due to an increased probability of depinning events during the drying process.[38] Under similar conditions of evaporation, Fig. 1b shows that the addition of motile bacteria does not appreciably affect the uniformity of the resulting stain. The similarity between the two cases can be ascribed to the fact that the motility of the bacteria (whose speed is $\approx 20~\mu m~s^{-1}$) is not enough to significantly affect the dynamics of the suspended particles away from the edge as these are subject to the net flow induced by the evaporation that drags them at a velocity of ≈ 10–$15~\mu m~s^{-1}$, similar to values previously reported in the literature.[7]

The effect of the bacteria on the particles becomes visible for slower evaporation rates (25 ± 5 minutes), when the flux flow induced by the evaporation process drags the particles at a velocity of ≈ 1–$2~\mu m~s^{-1}$, *i.e.* an order of magnitude smaller than the typical speed of motile bacteria. The evaporation rate was reduced by enclosing the evaporating droplet in a home-made chamber formed by two glass slides separated by a 400 μm parafilm spacer (see Fig. S3, ESI†). This geometry does not alter the flow pattern in the drying droplet, as shown by comparing the fast and slow evaporation of droplets of colloidal particles suspended in deionized water (see Fig. S1, ESI†). These droplets had same volume and particle concentration as those of the buffer solution employed in Fig. 1 (see Appendix). Thanks to this geometry, we were able to increase the local humidity in the droplet and thus extend its drying time in a controllable way up to 60 minutes. Under these slow evaporation conditions, the resulting stain is clearly different in the absence of the bacteria (Fig. 1c) and in their presence (Fig. 1d); in particular, the presence of motile bacteria produced a much more uniform

coffee disk stain[15] (see Supplementary Video 1, ESI†). This is a first indication that, as the droplet evaporation rate slows down, the presence of active matter can alter the deposition of particles during the drying process and, thus, the resulting stain.

To get more insight on the influence of motility, we analysed the dynamics occurring at the edge of the droplet in the initial stages of the evaporation process.[7,8] Because of the presence of active matter, the edge growth process becomes more irregular, and the resulting stain shows less spatial order and lacks close packing. In Fig. 2 we show a magnified view of a portion of the external boundary of the droplet, which is representative of the general appearance of the entire boundary. As shown in Fig. 2a, the accumulation of particles at the border in the buffer solution without bacteria produces a border that is continuous and compact featuring hexagonal packing;[39] furthermore, the trajectories in Fig. 2a show that the particles go straight to the border due to the evaporation flows and, once they reach it, they remain there forming a close-packed structure. Therefore, the boundary grows steadily with little rearrangement of the particles once they reach it (see left panel in Supplementary Video 2, ESI†). As shown in Fig. 2b, in the presence of motile bacteria, the resulting border shows instead a more jagged internal contour. Regions where the particles are tightly packed are still present, but when they form they are often subject to fast rearrangement, and they can even get disassembled by the action of motile bacteria passing nearby. The boundary presents active dynamics: as can be seen from the trajectories of the particles in Fig. 2b, after reaching the boundary, they still have a high probability of subsequently detaching from it pushed by the motile bacteria, and thus of rearranging the deposit under formation.

To check whether these differences in dynamics were due to the motility of the bacteria or to some other factors like their steric occupation of the space, we repeated the experiment with non-motile bacteria. In particular, we used bacteria that had stopped being motile as a consequence of the reduction of
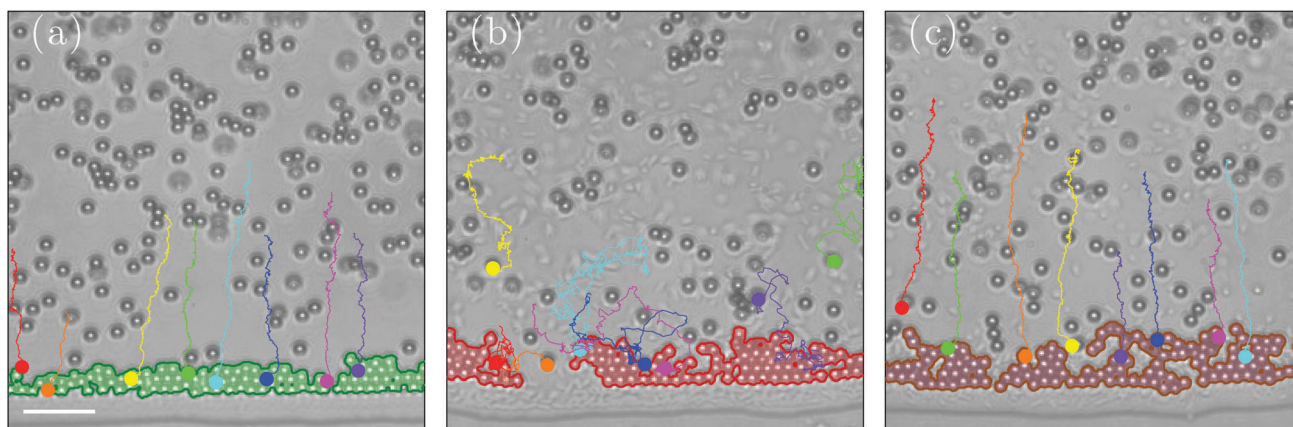

Fig. 2 Growth dynamics at the edge of drying droplets. Edge of a drying droplet of motility buffer containing (a) only colloidal particles, (b) colloidal particles and motile bacteria, and (c) colloidal particles and non-motile bacteria. The shaded area represents the already formed border, and the solid lines show the trajectories of some particles recorded over the preceding 60 s. In (b), because of the presence of motile bacteria, the particle trajectories are more complex and also feature events where a particle escapes the boundary after having reached it. The scalebar corresponds to 20 μm. See also Supplementary Videos 2, 3 and 4 (ESI†).

nutrients and oxygen in the buffer over time. In this case, shown in Fig. 2c (see also right panel in Supplementary Video 2, ESI†), the microscopic profile of the border shows more irregularities than in the case without bacteria (Fig. 2a), because of the presence of regions where non-motile bacteria accumulate. These regions, formed because of the accumulation of non-motile bacteria, cannot be entered by the colloidal particles, which leads at later stages to the formation of regions of the boundary that are devoid of colloidal particles. However, from the point of view of the edge growth dynamics, particles are deposited at the border and do not detach at a later stage, so that the area of the boundary increases steadily with no re-organisation of the position of the colloids within the edge, as in the case without bacteria shown in Fig. 2a.

We remark also that, in the presence of bacteria (Fig. 2b and c), the accumulation of bacteria between the droplet's contact

line and the edge formed by the colloidal particles is due to the fact that bacteria are smaller than the particles. Thus, they can fit in the narrow volume between the contact line and the first row of particles. Once bacteria reach this region, they often remain trapped there. In the presence of motile bacteria (Fig. 3b), the edge does not form continuously, but often features some gaps. These gaps allow more bacteria to reach the contact line in the initial phases of the edge formation. Instead, in the presence of non-motile bacteria (Fig. 3c), a continuous edge is formed much earlier during the evaporation process, preventing more bacteria from reaching the contact line.

Interestingly, in the presence of motile bacteria (Fig. 2b), we observe that particles are pushed by the bacteria in all directions, sometimes even away from the border. Thus, some particles exit the field of view opposite to the border in the presence of motile
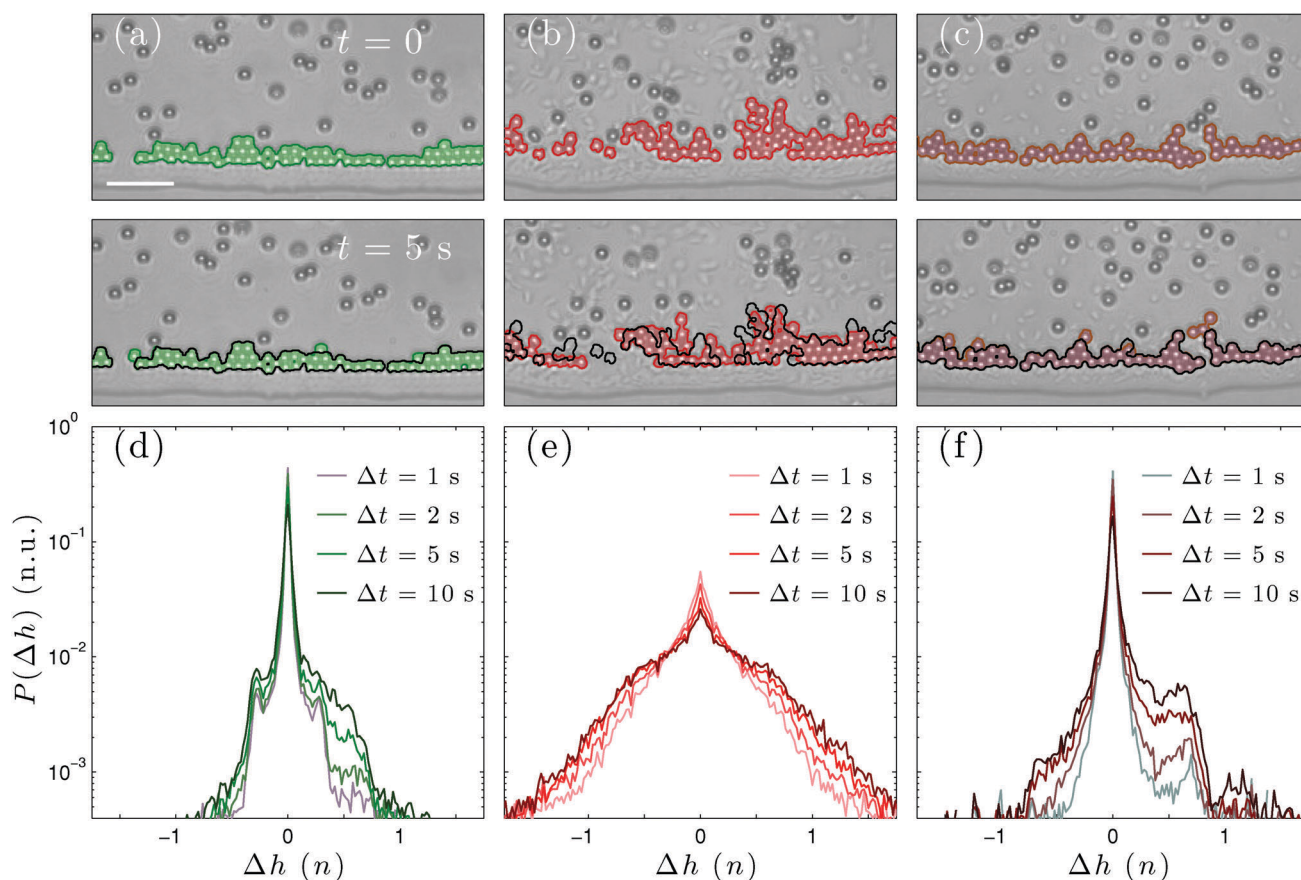

Fig. 3 Edge growth. (a–c) Two snapshots of the droplet's edge separated by a time lag $\Delta t = 5$ s for the cases of a drying droplet containing (a) only colloidal particles, (b) colloidal particles and motile bacteria, and (c) colloidal particles and non-motile bacteria. The shaded areas represent the border already formed at each time. The black solid lines in the bottom panels reproduce the border in the respective top panels to ease comparison. (a) Without bacteria and (c) with non-motile bacteria, the boundary grows only because new particles deposit and no particles detach from it over time, while, (b) with motile bacteria, the boundary changes shape in a more dynamic way as particles, after arriving at the boundary, keep moving and can even detach from it. The scalebar corresponds to 20 μm. (d–f) Distributions of the change of the boundary height (measured in numbers of particle layers in a close-packed border, so that $\Delta h = 1$ means that the border has grown by one particle) for time intervals $\Delta t = 1$, 2, 5 and 10 s for the cases of a drying droplet containing (d) only colloidal particles, (e) colloidal particles and motile bacteria, and (f) colloidal particles and non-motile bacteria. (d) Without bacteria and (f) with non-motile bacteria, the distribution decays fast away from zero and is characteristically asymmetric presenting a second smaller peak in the positive values indicating that the boundary height tend to increase, while, (e) with motile bacteria, the distribution is significantly broader and more symmetric around zero, indicating that the average height of the boundary can both increase or decrease (at least in the initial phases of the evaporation) as particles can be added to or removed from the boundary. See also Supplementary Video 2 (ESI†). More details about the procedure to construct the distributions of the spatial variation of the border height over a given time interval from the experimental data are given in the Appendix.

bacteria (see Supplementary Video 3, ESI†), while in the cases of the buffer solution with no bacteria and with non-motile bacteria, this never happens (see Supplementary Video 4, ESI†).

3 Analysis of the edge growth dynamics

In order to make these qualitative observations on the growth dynamics of the boundary more quantitative, we analysed the change in the edge height over time in the first 5 minutes from the initial formation of the boundary (Fig. 3). At each instant, we determined the boundary shape by identifying the clusters of particles close to the edge of the droplet. Fig. 3a–c show two such shapes at two instants separated by a time lag $\Delta t = 5$ s (see also Supplementary Video 2, ESI†) for the case without bacteria (Fig. 3a), with motile bacteria (Fig. 3b) and with non-motile bacteria (Fig. 3c). While in Fig. 3a and c, the boundary grows due to a steady deposition of additional particles over the previous boundary line, in Fig. 3b the boundary is dynamically changing and rearranging over time as new particles arrive, thus reducing the similarity between the boundaries captured at different times. This information is quantitatively represented by the distributions of the spatial variation of the border height over a given time interval in Fig. 3d–f. These distributions were calculated by measuring the change of the boundary height for different time lags $\Delta t = 1, 2, 5$ and 10 s to show how the border evolves over a given time interval. More details about the procedure to construct the distributions of the spatial variation of the border height over a given time interval from the experimental data are given in the Appendix. Without bacteria (Fig. 3d) and with non-motile bacteria (Fig. 3f), the distribution is narrow and skewed towards the positive side, confirming that the border is steadily growing due to the addition of new particles that immediately reach their final position and then do not undergo further rearrangement. With motile bacteria (Fig. 3e), the distribution is broader and more symmetric with similar likelihoods of both positive and negative values, indicating that the deposition of a particle and the escape of a particle are similarly likely within a short timeframe.

Qualitative information about the dynamics at the edge can also be extracted by analysing trajectories of individual particles once they reached the border for the cases without bacteria (Fig. 4a), with motile bacteria (Fig. 4b), and with non-motile bacteria (Fig. 4c). An ideal tool to do this is to estimate their average mean square displacements (MSDs), which we calculated on 300 s-long trajectories. For reference, the dashed lines in Fig. 4a–c represent the theoretical MSD for a Brownian particle of the same dimension ($2R = 3$ μm) in the bulk of an aqueous solution. In the presence of motile bacteria (Fig. 4b), the average MSD is about two orders of magnitude larger than in the absence of bacteria (Fig. 4a) or in the presence of non-motile bacteria (Fig. 4c). In particular, the MSD in the presence of bacteria (red solid line in Fig. 4b) shows superdiffusive behaviour (*i.e.* its slope is larger than 1) and is consistently above the reference of a passive Brownian particle (black dashed line); this is due to the fact that, after reaching the boundary, the particle on average leaves the boundary and behaves again as an active Brownian particle, before being dragged to the boundary again by the capillary flow, repeating this process a conspicuous number of times. This is strikingly different from the case without bacteria (Fig. 4a) or with non-motile bacteria (Fig. 4c), when the MSD shows subdiffusive behaviour and is below the reference MSD for a Brownian particle, indicating that, after an initial positional adjustment upon reaching the boundary, the particles are mainly stuck at a fix position.
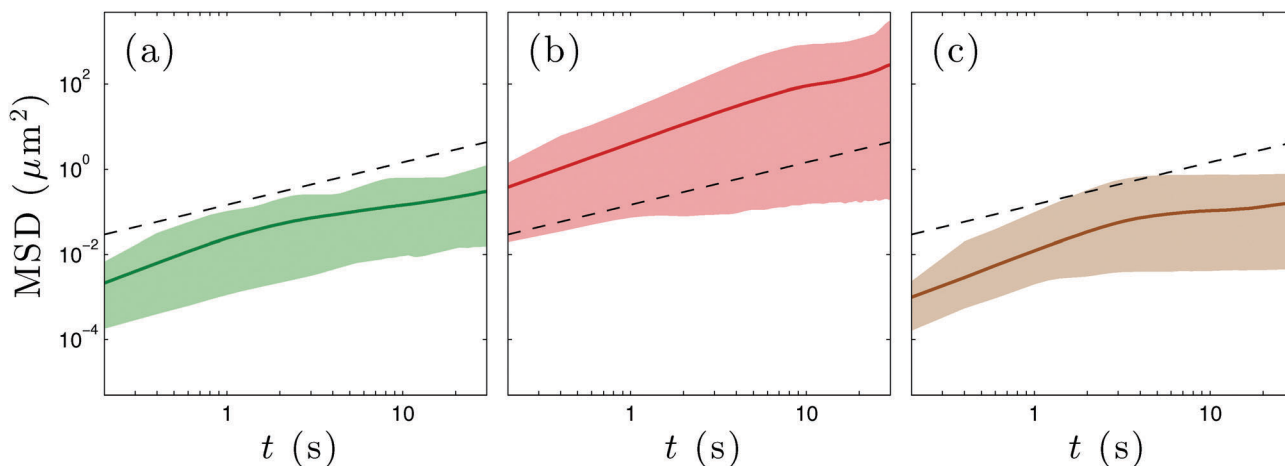

Fig. 4 Average mean square displacements (MSDs) of the particles after reaching the boundary. MSDs of ∼30 particles from the moment they reach the boundary for the cases of a drying droplet containing (a) only colloidal particles, (b) colloidal particles and motile bacteria, and (c) colloidal particles and non-motile bacteria. The solid lines represent the average MSDs and the shaded areas correspond to one standard deviation around the mean values. The black dashed lines represents the reference diffusive MSD for a Brownian particle in the bulk of an aqueous solution. (a) Without bacteria and (c) with non-motile bacteria, the motion of the particles is subdiffusive as the particles eventually settle within the boundary, as shown by the plateau at long time lags, while, (b) with motile bacteria, the particles perform active Brownian motion even after having reached the boundary, featuring superdiffusive motion at small time differences and enhanced diffusion at longer time differences.
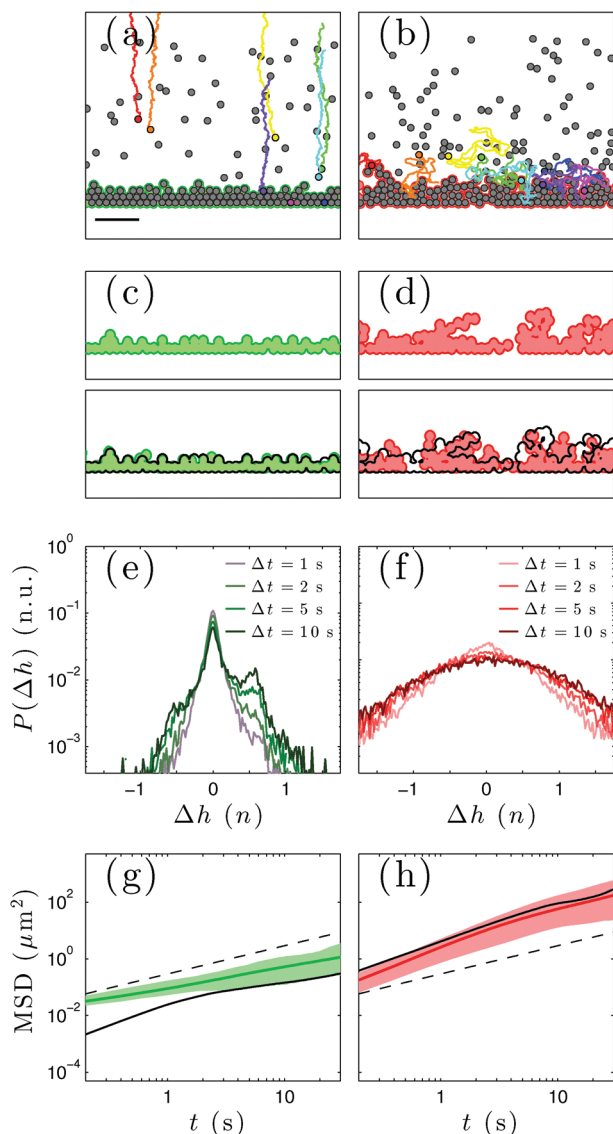
Fig. 5 Numerical simulations. The Brownian-dynamics simulation of the deposition of (a) passive and (b) active Brownian particles reproduces the features seen in Fig. 2: (a) the particles get deposited along straight trajectories on the border which grows with crystalline close-packing for passive particles, while (b) active particles feature more complex trajectories, leading to a less ordered border. The scalebar corresponds to 20 μm. (c and d) The boundary growth, (e and f) the distribution of the change of the boundary height, and (g and h) the mean square displacement (MSD) are also quantitatively similar to the experimental results provided in Fig. 3(a−f) and 4, respectively. In (g and h), the black solid lines represent the MSD measured experimentally in the cases without bacteria (Fig. 4a) and with motile bacteria (Fig. 4b), respectively. See also Supplementary Video 5 (ESI†).

4 Numerical simulations

In order to understand the dynamics of the boundary formation more deeply and to test its generality, we have developed a minimalistic numerical model capable of reproducing the key experimental observations and results. We describe the colloids in the drying droplet without bacteria as passive Brownian particles subject to a constant dragging force from the center

to the edge of the droplet. We assume these particles to be hard-spheres to prevent particle overlapping. As we are in an over-damped regime, we assume that the effect of this force on the dynamics of the particle is a constant drift velocity for each Brownian particle in the lower vertical direction. We assume the boundary of the droplet to be a straight line in the horizontal direction and the dragging force to be perpendicular to the boundary in the vertical direction. We describe the particles in a droplet with bacteria as active Brownian particles, so that, in addition to the features described above, the particles also have a constant propulsion velocity in a direction that changes randomly on a time scale determined by an effective rotational diffusion time $\tau_r = D_r^{-1} \approx 5$ s, where D_r is the particle rotational diffusion.[40] The results of the simulations have been analyzed following the same procedure described for the experimental acquisitions, and the outcome is summarised in Fig. 5 (see also Supplementary Video 5, ESI†). The left column represents the case of passive Brownian particles, and the right column represents the case of active Brownian particles. Overall, the results of our simulations reproduce well the main experimental observations both in terms of distributions of the change of the boundary height and in terms of the average MSD of the particles after reaching the boundary.

5 Conclusions

In conclusion, we have demonstrated that the presence of active matter can dramatically influence the growth dynamics at the border of an evaporating droplet and the resulting stain. In particular, we have shown that the effects due to the presence of active matter arise when the fluxes induced by the drying drag the suspended particles at a velocity that is low enough for the activity to have effect, and, therefore, they become particularly relevant for slowly drying droplets. Furthermore, our observations can help understand how bacteria and other motile microorganisms can adapt to environments that undergo periodic drying through their mobility. The possibility of influencing the coffee ring effect with active matter is not only relevant for several biophysical phenomena, such as the formation of biofilms and the spreading of pathogens in environments subject to periodic drying, but also for technological applications in printing,[41] coating,[42] thin film deposition,[43,44] self-assembly of nanostructures,[45–47] where active matter could become an additional degree of freedom to dynamically control these processes.[48,49]

Conflicts of interest

There are no conflicts of interest to declare.

Appendix A. Materials and methods

A.1 Experimental setup

The experiments were performed on a home-built inverted microscope capable of imaging the full basal view, the magnified basal view and the side view of the evaporating droplet by digital

video microscopy simultaneously (see Fig. S2, ESI†). The magnified view of the evaporating droplet near the contact line was imaged using a microscope objective ($40\times$, NA = 0.65) on a monochrome CMOS camera (Thorlabs, Germany) with an acquisition rate 5 fps. The full view of the evaporating droplets was imaged using a microscopic objective ($4\times$, NA = 0.13) pointing toward the CMOS camera (Thorlabs, Germany) with an effective magnification of $\approx 1.6\times$. For the side view, another microscopic objective ($10\times$, NA = 0.30) and a convex lens with a focal length of 35 mm were used with the CMOS camera (Thorlabs, Germany). For illumination, an incoherent white light lamp was directly projected onto the deposited droplets. The schematic of the experimental setup is shown in Fig. S2 (ESI†). The typical duration of an experiment was ≈ 5 minutes (for normal evaporation) and ≈ 30–60 minutes (for slow evaporation). In order to image a high resolution full view (Fig. 1) of the dried droplet (after evaporation), we used a combination of two convex lenses (focal lengths 50.0 mm and 100.0 mm) whose effective magnification corresponds to $\approx 0.58\times$.

A.2 Sample preparation

The experiments have been conducted using PS particles of 3.00 ± 0.07 μm diameter (Microparticles GmbH, Lot: PS-R-L2876) at a concentration of $\phi = 0.0055$ (volume fraction). For the evaporation process, we used glass microscope slides from Sail Brand (Ground edges 25.4 × 76.2 mm × 1 mm thick). The slides were cleaned with acetone and isopropanol before being immersed in a NaOH (0.25 M) bath for *ca.* 5 min to create a hydrophilic surface. At the beginning of each data acquisition, a droplet of colloidal solution was deposited on the slide. Typically, a droplet (0.6 μl) evaporates in about 5 min. To observe the effects of the presence of active particles, we had to slow down the evaporation process. To this aim a second glass slide was put on top of the sample at a distance of 400 μm by means of four layers of parafilm. The typical dimensions of a droplet were obtained from its side view and can be approximated by a spherical cap of ≈ 2.5 mm in diameter and ≈ 190 μm in height; therefore there is no risk of contact with the second glass slide put on top of the sample to slow down the evaporation process. The inner chamber is $\approx 10 \times 10$ mm (see Fig. S3, ESI†) and it is not sealed, as four holes are cut in the parafilm layers in order to keep the humidity inside the chamber higher than in the surrounding environment. In this configuration, we could extend the drying time to 35 min or longer (up to 1 hour). The lack of appreciable differences in the formation of the coffee ring stains for a water droplet containing PS particles under either fast or slow evaporation (see Fig. S1, ESI†) indicates that the presence of the chamber does not alter the flow patterns within the evaporating droplets, just their strength.

A.3 Bacteria growth protocol and preparation of motility buffer solution containing bacteria

Bacteria cells (*Escherichia coli*)[31,50] were cultured from the wild-type strain, RP437[50] provided by the *E. coli* Stock Center at Yale University. The liquid culture of RP437 was taken from a -80 °C archive stock and streaked onto a sterile hard agar medium. The inoculated agar plate was incubated and grown overnight at 32.5 °C. Single colonies grown upon agar were isolated by sterile toothpicking and inoculated into fresh liquid growth medium containing tryptone broth (1% tryptone). After reaching the saturation phase, the culture was diluted 1 : 100 into fresh tryptone broth. The final dilution was incubated at 32.5 °C and mildly shaken at 180 rpm until the culture reached its mid-exponential growth phase (OD600 ≈ 0.40). Then, a 7 ml volume of the final dilution was transferred into a falcon tube and centrifuged at 2000 rpm, 24 °C for 10 min. Precipitated RP437 pellets were then gently harvested and immersed in 5 mL of motility buffer containing 10 mM monobasic potassium phosphate (KH_2PO_4), 0.1 mM EDTA, 10 mM dextrose(glucose) and 0.002% of Tween 20.[32] This cell washing procedure was repeated two times in order to undermine the growth medium and halts further cell growth inside the motility buffer. Following this protocol, we obtained roughly 10^8 cells ml^{-1} in the final buffer.

The solution containing non-motile bacteria is obtained by waiting a sufficient amount of time, so the nutrients in the solution are exhausted and the amount of oxygen dissolved in the solution becomes smaller. In such conditions of starvation and low oxygen, *E. coli* become non-motile. The concentration of bacteria in the solution is constant in all the experiments.

A.4 Preparation of the solution containing polystyrene particles

In the case of polystyrene particles suspended in a buffer solution without bacteria, 58 μl of original PS particle solution (Microparticles.de) was added into 942 μl of buffer solution, prepared as described above. In the case of polystyrene particles suspended in a buffer solution containing bacteria, we took 58 μl of PS particles and added it to 942 μl of buffer solution containing bacteria, prepared as described above. From this solution, we took each time 0.6 μl for performing the experiments with motile and non-motile bacteria. To inspect the behaviour of PS particles in water, 58 μl of PS particles solution was added to 942 μl of deionized water (Milli-Q, resistivity: 18.2 MΩ cm) In all cases the final concentration of PS particles is the same, and it is equal to a volume fraction $\phi = 0.0055$.

A.5 Method for the analysis of the edge growth dynamics

In order to quantify the qualitative observations about the growth dynamics of the boundary provided in Fig. 3 and 5, we studied the distribution of the spatial variation of the boundary height occurring during the initial stages of the boundary formation. If we choose a time interval Δt of the order of 1–10 s and we observe how the shape of the boundary changes between frames separated by Δt, we can see a difference in the dynamics of the growth process of the different cases shown in Fig. 2. In fact, in a time interval of the order of 5–10 s, there is on average a net deposition of a few particles over the visible boundary in the cases with no bacteria and with non-motile bacteria. In the case with motile bacteria, in 5–10 s the boundary typically experiences the deposition of some new particles, the detachment of some particles, and the re-organization of the particles already present in the boundary. In order to statistically compare the boundary variations

over a given time interval, we first calculated the distributions for each couple of frames separated by that time interval, and then we averaged such distributions.

Here we explain how we proceeded to obtain, from the experimental movies, the distributions shown in Fig. 3d–f of the main manuscript. Details of the procedure are illustrated in Fig. S4 (ESI†). For each frame we isolate the region constituting the external boundary (Fig. S4a, showing a region of 800 pixels wide corresponding to about 120 μm, ESI†). From the set of pixels representing the boundary in the image, we build a boundary profile by counting the number of pixels belonging to the boundary for each given pixel column constituting the image, obtaining the profile shown in Fig. S4c (ESI†). We section this profile in non-overlapping columns of $R_0 = 10$ pixels width (the original image is 1024×1024 pixels, we discard each time the most external 12 pixels closest to the image boundary), corresponding, in our case, to 1.5 μm, *i.e.*, the radius of a PS particle. For each column, we calculate the height of the rectangle in such a way that its area is the same as the area of the profile area in the column (Fig. S4d, ESI†). We proceed with the subsequent analysis representing the complete boundary isolated in each frame by its sectioned equivalent shown in Fig. S4e (ESI†). Therefore, for each frame, we have a sequence of columns (all frames are sectioned in exactly the same way), and for each column we have its area: if j indicates the frame, and i represents the column, then the boundary is represented by a function $A_j(i)$. The area of a column can be calculated in units of areas of one particle: so, if $R_0 = 10$ pixels corresponds to a particle radius in the image, then $a_0 = \pi R_0^2$ is the number of pixels occupied by the image of one particle, and we will express $A_j(i)$ by the number of particles that would cover an equivalent area in pixels.

To quantify the growth dynamics of the boundary edge, we investigate how the boundary changes with time and in particular how the function $A_j(i)$ varies on a given time interval. Therefore, we chose a time interval Δt of the order of few seconds ($\Delta t = 1, 2, 5, 10$ s, corresponding to a difference of $\Delta j = 5, 10, 25, 50$ frames at an acquisition rate of 5 fps) and we calculate the boundary variation $\Delta h_j(i) = A_{j+\Delta j}(i) - A_j(i)$. We calculate P_j as the distribution of the values of Δh_j over the various columns. In principle, Δh_j can assume positive and negative values, depending on whether the boundary is growing or shrinking, so we define the distribution P_j over a domain centred in 0, representing the possible values of Δh_j. The distribution $P(\Delta h)$ represented in Fig. 3d–f is the average on all the considered frames j of the frame distributions P_j. We note that the plots in Fig. 3d–f are in logarithmic scale in the ordinate axis.

Acknowledgements

Notes and references

1 R. Brown, *Philos. Mag.*, 1829, **6**, 161–166.
2 R. E. Goldstein, *Phys. Today*, 2018, **71**, 32–38.
3 R. D. Deegan, O. Bakajin, T. F. Dupont, G. Huber, S. R. Nagel and T. A. Witten, *Nature*, 1997, **389**, 827–829.
4 R. D. Deegan, O. Bakajin, T. F. Dupont, G. Huber, S. R. Nagel and T. A. Witten, *Phys. Rev. E: Stat. Phys., Plasmas, Fluids, Relat. Interdisc. Top.*, 2000, **62**, 756–765.
5 R. D. Deegan, *Phys. Rev. E: Stat. Phys., Plasmas, Fluids, Relat. Interdisc. Top.*, 2000, **61**, 475–485.
6 H. Hu and R. G. Larson, *Langmuir*, 2005, **21**, 3963–3971.
7 Á. G. Marn, H. Gelderblom, D. Lohse and J. H. Snoeijer, *Phys. Rev. Lett.*, 2011, **107**, 085502.
8 P. J. Yunker, D. J. Durian and A. G. Yodh, *Phys. Today*, 2013, **66**, 60–61.
9 B. M. Weon and J. H. Je, *Phys. Rev. Lett.*, 2013, **110**, 028303.
10 H. M. van der Kooij, G. T. van de Kerkhof and J. Sprakel, *Soft Matter*, 2016, **12**, 2858–2867.
11 B. M. Weon and J. H. Je, *Phys. Rev. E: Stat., Nonlinear, Soft Matter Phys.*, 2010, **82**, 015305.
12 P. J. Yunker, T. Still, M. A. Lohr and A. G. Yodh, *Nature*, 2011, **476**, 308–311.
13 V. H. Chasatia and Y. Sun, *Soft Matter*, 2011, **7**, 10135–10143.
14 T. A. H. Nguyen, M. A. Hampton and A. V. Nguyen, *J. Phys. Chem. C*, 2013, **117**, 4707–4716.
15 P. J. Yunker, M. A. Lohr, T. Still, A. Borodin, D. J. Durian and A. G. Yodh, *Phys. Rev. Lett.*, 2013, **110**, 035501.
16 H. Hu and R. G. Larson, *J. Phys. Chem. B*, 2006, **110**, 7090–7094.
17 Y.-F. Li, Y.-J. Sheng and H.-K. Tsao, *Langmuir*, 2013, **29**, 7802–7811.
18 T. Still, P. J. Yunker and A. G. Yodh, *Langmuir*, 2012, **28**, 4984–4988.
19 W. Sempels, R. De Dier, H. Mizuno, J. Hofkens and J. Vermant, *Nat. Commun.*, 2013, **4**, 1757.
20 A. Marin, R. Liepelt, M. Rossi and C. J. Kähler, *Soft Matter*, 2016, **12**, 1593–1600.
21 S. N. Varanakkottu, M. Anyfantakis, M. Morel, S. Rudiuk and D. Baigl, *Nano Lett.*, 2016, **16**, 644–650.
22 R. Malinowski, G. Volpe, I. P. Parkin and G. Volpe, *J. Phys. Chem. Lett.*, 2018, **9**, 659–664.
23 C. Ott, R. Bruce and D. Pierson, *Microb. Ecol.*, 2004, **47**, 133–136.
24 T. T. Nellimoottil, P. N. Rao, S. S. Ghosh and A. Chattopadhyay, *Langmuir*, 2007, **23**, 8655–8658.
25 D. Yanni, A. Kalziqi, J. Thomas, S. L. Ng, S. Vivek, W. C. Ratcliff, B. K. Hammer and P. J. Yunker, 2017, arXiv:1707.03472, 1–12.
26 A. Susarrey-Arce, A. Marin, A. Massey, A. Oknianska, Y. Diaz-Fernandez, J. F. Hernández-Sánchez, E. Griffiths, J. G. E. Gardeniers, J. H. Snoeijer, D. Lohse and R. Raval, *Langmuir*, 2016, **32**, 7159–7169.
27 A. Susarrey-Arce, J. F. Hernández-Sánchez, M. Marcello, Y. Diaz-Fernandez, A. Oknianska, I. Sorzabal-Bellido, R. Tiggelaar, D. Lohse, H. Gardeniers, J. Snoeijer, A. Marin and R. Raval, *ACS Appl. Bio Mater.*, 2018, **1**, 1294–1300.
28 G. A. Turnbull, J. A. W. Morgan, J. M. Whipps and J. R. Saunders, *FEMS Microbiol. Ecol.*, 2001, **36**, 21–31.

29 C. Matz and K. Jürgens, *Appl. Environ. Microbiol.*, 2005, **71**, 921–929.

30 M. Hennes, J. Tailleur, G. Charron and A. Daerr, *Proc. Natl. Acad. Sci. U. S. A.*, 2017, 201703997.

31 H. C. Berg, *E. coli in Motion*, Springer-Verlag, 2004.

32 E. Pinçe, S. K. P. Velu, A. Callegari, P. Elahi, S. Gigan, G. Volpe and G. Volpe, *Nat. Commun.*, 2016, **7**, 10907.

33 G. Miño, T. E. Mallouk, T. Darnige, M. Hoyos, J. Dauchet, J. Dunstan, R. Soto, Y. Wang, A. Rousselet and E. Clement, *Phys. Rev. Lett.*, 2011, **106**, 048102.

34 A. Morozov and D. Marenduzzo, *Soft Matter*, 2014, **10**, 2748–2758.

35 A. Argun, A.-R. Moradi, E. Pinçe, G. B. Bagci, A. Imparato and G. Volpe, *Phys. Rev. E*, 2016, **94**, 062150.

36 https://microparticles.de/en/eigenschaften, PS microspheres have an anionic charge and are hydrophobic, and the surface functional group is sulfate.

37 J. Schwarz-Linek, J. Arlt, A. Jepson, A. Dawson, T. Vissers, D. Miroli, T. Pilizota, V. A. Martinez and W. C. K. Poon, *Colloids Surf., B*, 2016, **137**, 2–16.

38 K. Sefiane, *J. Colloid Interface Sci.*, 2004, **272**, 411–419.

39 X. Xu, L. Ma, D. Huang, J. Luo and D. Guo, *Colloids Surf., A*, 2014, **477**, 28–31.

40 G. Volpe, S. Gigan and G. Volpe, *Am. J. Phys.*, 2014, **82**, 659–664.

41 M. Ikegawa and H. Azuma, *JSME Int. J., Ser. B*, 2004, **47**, 490–496.

42 K. A. Baldwin, M. Granjard, D. I. Willmer, K. Sefiane and D. J. Fairhurst, *Soft Matter*, 2011, **7**, 7819–7826.

43 X. Zhang, A. Crivoi and F. Duan, *Sci. Rep.*, 2015, **5**, 10926.

44 C. N. Kaplan and L. Mahadevan, *J. Fluid Mech.*, 2015, **781**, 1–13.

45 E. Rabani, D. R. Reichman, P. L. Geissler and L. E. Brus, *Nature*, 2003, **426**, 272–274.

46 A. Suhendi, A. B. D. Nandiyanto, M. M. Munir, T. Ogi, L. Gradon and K. Okuyama, *Langmuir*, 2013, **29**, 13152–13161.

47 S. Ni, J. Leemann, I. Buttinoni, L. Isa and H. Wolf, *Sci. Adv.*, 2016, **2**, e1501779.

48 R. Ni, M. A. Cohen Stuart and M. Dijkstra, *Nat. Commun.*, 2013, **4**, 2704.

49 C. Reichhardt and C. J. Olson Reichhardt, *Phys. Rev. E: Stat., Nonlinear, Soft Matter Phys.*, 2015, **91**, 032313.

50 J. S. Parkinson, *J. Bacteriol.*, 1978, **135**, 45–53.